

# Nonmonotonic magnetoresistance of a two-dimensional viscous electron-hole fluid in a confined geometry

P.S. Alekseev,<sup>1</sup> A.P. Dmitriev,<sup>1</sup> I.V. Gornyi,<sup>2,3,1,4</sup> V.Yu. Kachorovskii,<sup>1,4,2</sup> B.N. Narozhny,<sup>3,5</sup> and M. Titov<sup>6,7</sup>

<sup>1</sup>*A.F. Ioffe Physico-Technical Institute, 194021 St. Petersburg, Russia*

<sup>2</sup>*Institut für Nanotechnologie, Karlsruhe Institute of Technology, 76021 Karlsruhe, Germany*

<sup>3</sup>*Institut für Theorie der kondensierten Materie, Karlsruhe Institute of Technology, 76128 Karlsruhe, Germany*

<sup>4</sup>*L.D. Landau Institute for Theoretical Physics, Kosygina street 2, 119334 Moscow, Russia*

<sup>5</sup>*National Research Nuclear University MEPhI (Moscow Engineering Physics Institute), 115409 Moscow, Russia*

<sup>6</sup>*Radboud University Nijmegen, Institute for Molecules and Materials, NL-6525 AJ Nijmegen, The Netherlands*

<sup>7</sup>*ITMO University, 197101 St. Petersburg, Russia*

(Dated: June 11, 2018)

Ultra-pure conductors may exhibit hydrodynamic transport where the collective motion of charge carriers resembles the flow of a viscous fluid. In a confined geometry (e.g., in ultra-high quality nanostructures) the electronic fluid assumes a Poiseuille-like flow. Applying an external magnetic field tends to diminish viscous effects leading to large negative magnetoresistance. In two-component systems near charge neutrality the hydrodynamic flow of charge carriers is strongly affected by the mutual friction between the two constituents. At low fields, the magnetoresistance is negative, however at high fields the interplay between electron-hole scattering, recombination, and viscosity results in a dramatic change of the flow profile: the magnetoresistance changes its sign and eventually becomes linear in very high fields. This novel non-monotonic magnetoresistance can be used as a fingerprint to detect viscous flow in two-component conducting systems.

The independent particle approximation<sup>1,2</sup> has dominated the solid state physics for nearly a century. While clearly successful in describing most of the basic transport phenomena in metals and semiconductors, this approach completely neglects Coulomb interaction between charge carriers (the latter is frequently said to be justified by the “weakness” of electron-electron interaction due to, e.g., screening or statistical effects). To be more specific, in many conventional conductors the typical interaction length scale,  $\ell_{ee}$ , is too long in comparison to other relevant scales in the system. In particular, at low temperatures the dominant scattering process is due to potential disorder and hence the shortest length scale is the mean free path,  $\ell_{\text{dis}} \ll \ell_{ee}$ , which determines the residual Drude resistivity at  $T = 0$ . At high temperatures, the electron-phonon interaction dominates,  $\ell_{ph} \ll \ell_{ee}$ . If these two temperature regimes overlap, then indeed (at least, away from any phase transitions) the role of electron-electron interaction is reduced to small corrections. However, if there exists a temperature window where  $\ell_{ee} \ll \ell_{\text{dis}}, \ell_{ph}$ , then in that case the independent particle approximation is violated: the motion of charge carriers becomes collective (or hydrodynamic) and hence transport properties of the system are determined by interaction<sup>3</sup>.

Signatures of the hydrodynamic behavior have been observed in recent experiments in graphene<sup>4–6</sup> and palladium cobaltate<sup>7</sup>. The effect of external magnetic field on electronic transport in systems with  $\ell_{ee} \lesssim \ell_{\text{dis}}, \ell_{ph}$  was studied in magnetotransport measurements in ultra-high-mobility GaAs quantum wells<sup>8–10</sup> and more recently in the Weyl semimetal WP<sub>2</sub><sup>11</sup> reporting, in both cases, large negative magnetoresistance. A theoretical explanation of that effect has been recently suggested in Ref. 12 (see also Ref. 13) on the basis of a hydrodynamic model where

the viscosity coefficients are functions of temperature and magnetic field.

A detailed account of the history of magnetotransport measurements is beyond the scope of this paper. Here we only stress the following well known facts: at the single-particle level, there is no classical magnetoresistance (MR) in single-band (or one-component) systems; taking into account more than one band of carriers (e.g., in semiconductors) leads to the MR that is typically positive, quadratic ( $\sim B^2$ ) at low fields, and saturating at classically high fields (i.e., for  $\omega_c \tau \gg 1$ , where  $\omega_c$  is the cyclotron frequency and  $\tau$  is the disorder mean free time); in some particular cases, MR in strong fields does not saturate and may exhibit linear field dependence; and finally, in the majority of situations MR is positive, while the negative MR occurs only in special circumstances.

Nonsaturating MR has received considerable attention in recent literature. Large positive (and often linear) MR was reported in graphene and topological insulators close to charge neutrality<sup>14–22</sup>, Bi<sub>2</sub>Te<sub>3</sub> nanosheets<sup>23</sup>, a topological material LuPdBi<sup>24</sup>, semimetals WTe<sup>25,26</sup>, NbP<sup>27</sup>, LaBi<sup>28</sup>, Cd<sub>2</sub>As<sub>3</sub><sup>29</sup>, and multilayer graphene<sup>30</sup>. At the same time, negative MR was found in Weyl semimetals<sup>31,32</sup>, Dirac semimetals<sup>33</sup>, a novel semimetal TaAs<sub>2</sub> without Dirac dispersion<sup>34</sup>, and at the LaAlO<sub>3</sub>/SrTiO<sub>3</sub> interface<sup>35</sup>.

Observations of negative MR in Weyl semimetals have attracted substantial interest due to theoretical suggestions<sup>36–39</sup> that this effect could be a direct condensed matter manifestation of the Adler-Bell-Jackiw chiral anomaly<sup>40–42</sup>. However, the unexpected variety of materials exhibiting negative MR<sup>8–11,31–35</sup> does not support the idea that such measurements may provide a “smoking gun” for detecting a Weyl semimetal<sup>37,39</sup>. Rather, there may be several different mechanisms of

negative MR similarly to the case of linear positive MR that can appear, e.g., due to disorder<sup>19,43</sup>, in the extreme quantum limit<sup>24,44,45</sup>, or in compensated two-component systems<sup>20,22,46–49</sup>. In particular, the chiral anomaly manifests itself in the negative longitudinal MR<sup>32,36–39</sup> (i.e., the case of parallel electric and magnetic fields,  $\mathbf{B} \parallel \mathbf{E}$ ), while Ref. 11 reports negative transverse MR.

In this paper, we consider the effect of the perpendicular magnetic field on a two-dimensional (2D), two-component system of charge carriers in the hydrodynamic regime at charge neutrality. While the most obvious experimental realization of such system is monolayer graphene, we consider the simplest case of two parabolic bands. We believe that our qualitative results are independent of the particular form of the spectrum and hence our theory is equally applicable to bilayer graphene, topological insulators, or topological semimetals.

We show that in narrow rectangular samples (with the length much larger than the width,  $L \gg W$ ) a viscous electronic fluid exhibits a Poiseuille-like flow. The spatial profile of the current density in this flow is strongly affected by quasiparticle recombination, impurity scattering, and mutual friction between the two constituent subsystems (i.e., electron-hole scattering).

In the widest (in theoretical terms – infinite) samples, transport properties of the system are dominated by the impurity and (in the two-component case) electron-hole scattering. Both processes have a very similar effect leading to a finite Drude-like resistance. In narrower samples, viscous effects start playing a role. As a result, the flow becomes nonuniform. The typical scale of the spatial variation of the current density,  $\ell_G$ , comprises the viscosity and Drude mean free time. In the limit where this length exceeds the sample width,  $\ell_G \gg W$ , we recover the standard parabolic flow profile<sup>50,51</sup>. The corresponding resistance is then proportional to the viscosity. This is a manifestation of the Gurzhi effect<sup>52</sup> and therefore we refer to this length scale as the Gurzhi length. In our theory, the Gurzhi resistance exceeds the inviscid Drude resistance. Note, that this is not a contradiction to either the recent observation of super-ballistic flow in graphene<sup>6,53</sup> or the original Gurzhi effect<sup>52</sup>. The reason is that we are considering the electronic fluid in the hydrodynamic regime to begin with and do not compare it with a ballistic (Knudsen-like<sup>54</sup>) regime where the resistance is determined by the scattering off the system boundaries or large (macroscopic) obstacles.

In the samples wider than the Gurzhi length,  $W \gg \ell_G$ , the flow profile is modified: instead of the standard parabola we obtain a variant of the catenary curve. Significant changes of the current density are limited to a boundary layer of the size  $\ell_G$ , while deep in the bulk the flow is nearly uniform, as if in the infinite sample.

Finally, the electron-hole recombination tends to create its own boundary layer<sup>47,48,55</sup>. In this paper we consider the case of weak (or slow) recombination, such that the corresponding length scale is longer than the Gurzhi length,  $\ell_R > \ell_G$ . In the case where both length scales

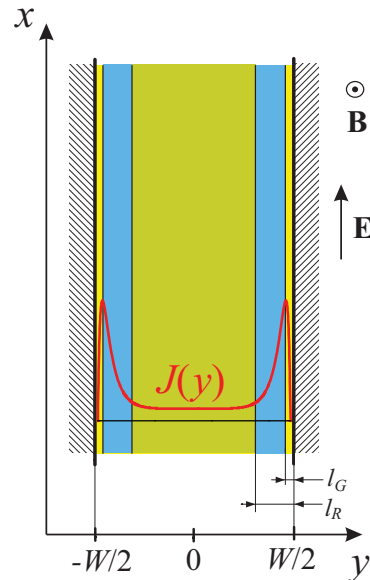


FIG. 1: Inhomogeneous flow profile resulting from the interplay of electron-hole recombination, viscosity, impurity scattering, and mutual friction between the two system constituents. The profile is given for the case  $W \gg \ell_R \gg \ell_G$ .

are much smaller than the sample width, the “recombination layer” is separated from the boundary by the smaller “Gurzhi layer”, see Fig. 1. These layers are characterized by a strongly inhomogeneous flow, in contrast to the bulk of the system where the flow is uniform.

In the inviscid fluid, quasiparticle recombination processes strongly affect the transport properties of the system leading to nonsaturating (at charge neutrality), linear positive MR in strong fields<sup>46–48</sup>. At the same time, viscous one-component systems are characterized by negative MR<sup>11,12</sup>. Here we show that neutral two-component systems may exhibit both types of behavior at the same time so that the MR is *non-monotonous*: in weak magnetic fields, we find the negative, parabolic MR, while in strong fields the resistance grows with the field eventually approaching the linear dependence.

Our results are relevant to a wide range of novel materials including compensated semimetals<sup>11</sup>, topological insulators, and multilayer graphenes. Our main qualitative conclusions are independent of the details of the quasiparticle spectrum and are applicable also to systems with the linear (Dirac) spectrum such as the monolayer graphene. As we specifically target the hydrodynamic, viscous flow of charge carriers, we implicitly assume the regime of relatively high temperatures (more precisely, our theory is justified in the “hydrodynamic” temperature window<sup>3</sup> with  $\ell_{ee} \ll \ell_{dis}, \ell_{ph}$ ). Under this assumption, all low-temperature quantum effects are washed out. In particular, Landau quantization plays no role and we may consider very large magnetic fields without running into quantum Hall physics.

## I. COMPENSATED SEMIMETALS IN TWO DIMENSIONAL STRIP GEOMETRY

Consider a two-component conductor (e.g., a narrow-band semiconductor or a semimetal) in 2D. Allowing for electron-hole recombination, the continuity equations for the two constituent densities can be written as

$$\frac{\partial \delta n_\alpha}{\partial t} + \nabla \cdot \mathbf{j}_\alpha = -\frac{\delta n_e + \delta n_h}{2\tau_R}, \quad (1)$$

where  $\alpha = e, h$  distinguishes the type of carriers,  $\delta n_\alpha$  are the deviations of the carrier densities from their equilibrium values  $n_\alpha^{(0)}$ ,  $\mathbf{j}_\alpha$  are the carrier currents, and  $\tau_R$  is the electron-hole recombination time.

Charge transport in such systems can be described by a set of macroscopic equations that are typically obtained by integrating the kinetic (Boltzmann) equation<sup>12,13,48</sup>. In the disorder-dominated regime such a theory can be reduced to a generalized Ohm's law. In contrast, in the collision-dominated – or *hydrodynamic* – regime the resulting macroscopic theory is a generalization of the standard Navier-Stokes equation<sup>50</sup>. In the simplest case of two symmetric parabolic bands<sup>56</sup>, the continuity equations for the momentum densities – or currents – of the two types of charge carriers are given by

$$\begin{aligned} \frac{\partial \mathbf{j}_\alpha}{\partial t} + \frac{\langle v^2 \rangle}{2} \nabla \delta n_\alpha - \frac{e_\alpha n_\alpha^{(0)}}{m} \mathbf{E} - \omega_\alpha [\mathbf{j}_\alpha \times \mathbf{e}_z] &= \quad (2) \\ &= -\frac{\mathbf{j}_\alpha}{\tau} - \frac{\mathbf{j}_\alpha - \mathbf{j}_{\alpha'}}{2\tau_{eh}} + \eta_{xx} \Delta \mathbf{j}_\alpha + \eta_{xy}^\alpha [\Delta \mathbf{j}_\alpha \times \mathbf{e}_z]. \end{aligned}$$

Here we consider the orthogonal magnetic field,  $\mathbf{B} = B\mathbf{e}_z$ ; the electron and hole charges are  $e_h = e > 0$ ,  $e_e = -e$ , and the cyclotron frequencies are  $\omega_\alpha = e_\alpha B / (mc) = \omega_c e_\alpha / e$ ; the index  $\alpha'$  denotes the constituent other than  $\alpha$ :  $\alpha' = e$  for  $\alpha = h$  and vice versa;  $\tau_{eh}$  is the momentum relaxation time due to electron-hole scattering; and the averaging (for the parabolic spectrum with the constant density of states  $\nu_0$ ) is defined as<sup>46</sup>

$$\langle \dots \rangle = -\int d\epsilon \frac{\partial f^{(0)}(\epsilon)}{\partial \epsilon} (\dots),$$

where  $f^{(0)}(\epsilon)$  is the Fermi distribution function. The two viscosities,  $\eta_{ij}$ , depend on the magnetic field<sup>12,57</sup>

$$\eta_{xx} = \eta_0 / (1 + 4\omega_c^2 \tau_{ee}^2), \quad \eta_{xy}^\alpha = 2\omega_\alpha \tau_{ee} \eta_{xx}, \quad (3)$$

where  $\eta_0$  is the shear viscosity in the absence of the magnetic field

$$\eta_0 = \langle v^4 \rangle \tau_{ee} / (4\langle v^2 \rangle) \sim \langle v^2 \rangle \tau_{ee}, \quad (4)$$

and  $\tau_{ee}$  is the electron-electron scattering time.

Our hydrodynamic approach is justified if the electron-electron scattering time  $\tau_{ee}$  is the shortest time scale in the problem (including the ‘‘ballistic’’ time defined by the sample width)

$$\tau_{ee} \ll \tau, \tau_R, \tau_{eh}, \tau_B, \quad \tau_B \sim W / \sqrt{\langle v^2 \rangle}. \quad (5)$$

In this case, the equations (2) describe the two (electron and hole) fluids that are weakly coupled by electron-hole scattering<sup>47,48</sup>. Unlike the single-component fluid considered in Ref. 12, these two fluids cannot be considered as incompressible. However, under the assumption (5) electron-hole recombination dominates the viscous compressibility (related to bulk viscosity) allowing us to drop the latter from Eqs. (2). In the inviscid case<sup>46,47</sup>, the recombination-induced compressibility leads to positive linear magnetoresistance in classically strong fields.

At charge neutrality, the currents and densities of the two constituents are not independent. Introducing the total quasiparticle density,  $\rho = n_e + n_h$  and the linear combinations of the two currents,  $\mathbf{P} = \mathbf{j}_e + \mathbf{j}_h$  and  $\mathbf{j} = \mathbf{j}_h - \mathbf{j}_e$ , we re-write the hydrodynamic theory (1) and (2) as

$$\frac{\partial \delta \rho}{\partial t} + \nabla \cdot \mathbf{P} = -\frac{\delta \rho}{\tau_R}, \quad \nabla \cdot \mathbf{j} = 0, \quad (6a)$$

$$\begin{aligned} \frac{\partial \mathbf{P}}{\partial t} + \frac{\langle v^2 \rangle}{2} \nabla \delta \rho - \omega_c [\mathbf{j} \times \mathbf{e}_z] &= -\frac{\mathbf{P}}{\tau} + \eta_{xx} \Delta \mathbf{P} \quad (6b) \\ &+ \eta_{xy} [\Delta \mathbf{j} \times \mathbf{e}_z]. \end{aligned}$$

$$\begin{aligned} \frac{\partial \mathbf{j}}{\partial t} - \frac{e\rho^{(0)}}{m} \mathbf{E} - \omega_c [\mathbf{P} \times \mathbf{e}_z] &= \quad (6c) \\ &= -\frac{\mathbf{j}}{\tau} - \frac{\mathbf{j}}{\tau_{eh}} + \eta_{xx} \Delta \mathbf{j} + \eta_{xy} [\Delta \mathbf{P} \times \mathbf{e}_z]. \end{aligned}$$

Here  $\eta_{xy} = \eta_{xy}^\alpha e_\alpha / e$  and  $\rho = \rho^{(0)} + \delta \rho$  with  $\rho^{(0)} = n_e^{(0)} + n_h^{(0)}$ .

Finally, we consider the strip geometry, i.e., narrow rectangular samples with the length,  $L$ , much larger than the width,  $W$ . In this case, all physical quantities are functions of the transverse coordinate  $y$ . At charge neutrality, the total electric field is equal to the applied field,  $\mathbf{E} = (E, 0)$ , which we assume to be homogeneous. Requiring that no current flows out of the sides of the sample,  $j_y(\pm W/2) = P_y(\pm W/2) = 0$ , we find that the electric current is directed along the strip,  $\mathbf{J} = e\mathbf{j} = e(j(y), 0)$ , while the total quasiparticle flow,  $\mathbf{P} = (0, P(y))$ , is orthogonal. Now we recall that in the hydrodynamic regime the macroscopic currents vary on length scales  $\xi$  that are much longer than any other length scale in the problem. Estimating the ratio of the Hall viscosity terms in Eqs. (6) to the Lorentz terms as  $\eta_{xx} \tau_{ee} / \xi^2 \ll 1$ , we neglect the former and arrive at the steady state equations

$$P' = -\delta \rho / \tau_R, \quad (7a)$$

$$\langle v^2 \rangle \delta \rho' / 2 + \omega_c j = -P / \tau + \eta_{xx} P'' \quad (7b)$$

$$-e\rho^{(0)} E / m - \omega_c P = -j / \tau - j / \tau_{eh} + \eta_{xx} j'' \quad (7c)$$

The above equations describe the linear response transport in the system in the hydrodynamic regime. Below we analyze their solutions and discuss the applicability of the results.

## II. RESULTS

### A. Infinite sample

Consider first the simplest case of an infinite sample. Here the currents are uniform and the solution to Eqs. (7) is trivial:

$$j = j_0 = \frac{\sigma_0 E}{1 + \omega_c^2 \tau \tau_*}, \quad P = -\omega_c \tau j_0 = -\frac{\sigma_0 E \omega_c \tau}{1 + \omega_c^2 \tau \tau_*}, \quad (8a)$$

where

$$\sigma_0 = e\rho^{(0)}\tau_*/m, \quad \tau_* = \tau\tau_{eh}/(\tau + \tau_{eh}). \quad (8b)$$

In the absence of magnetic field only the longitudinal electric current is flowing through the sample. The resistance is provided by the impurity scattering and mutual friction between the electron and hole subsystems. Once the field is applied, the lateral neutral quasiparticle flow appears. In the clean limit,  $\tau \gg \tau_{eh}$ ,  $1/\omega_c$ , the longitudinal electric current vanishes. If some disorder is present, then the result (8a) describes *positive* magnetoresistance.

### B. Finite-size sample without recombination

Now we consider a sample of finite width, but neglect the recombination processes. Then the continuity equation (7a) combined with the hard-wall boundary conditions,  $P(\pm W/2) = 0$ , yield the vanishing lateral flow,  $P = 0$ , while the equation (7c) for the current  $j$  has the form

$$\ell_G^2(B)j'' - j + \sigma_0 E = 0, \quad (9)$$

where  $\sigma_0$  is defined in Eq. (8b) and we have introduced the Gurzhi length [field-dependent by means of Eq. (3)].

$$\ell_G(B) = \sqrt{\eta_{xx}\tau_*} = \sqrt{\eta_0\tau_*}/\sqrt{1 + (2\omega_c\tau_{ee})^2}. \quad (10)$$

Assuming the standard hydrodynamic no-slip boundary conditions,  $j(\pm W/2) = 0$ , we find the catenary profile

$$j = \sigma_0 E \left[ 1 - \frac{\cosh y/\ell_G(B)}{\cosh W/[\ell_G(B)]} \right], \quad (11a)$$

with the total sample resistance

$$R = \frac{R_0}{1 - \frac{2\ell_G(B)}{W} \tanh \frac{W}{2\ell_G(B)}}, \quad R_0 = \frac{L}{e\sigma_0 W}. \quad (11b)$$

Here  $R_0$  is the sample resistance in the inviscid limit.

Assuming the large Gurzhi length,  $\ell_G(B) \gg W$ , we may expand the expression for the electric current (11a) and recover the parabolic profile typical of the standard Poiseuille flow<sup>50,51</sup>. In this case, the sample resistance is proportional to the shear viscosity (a manifestation of the Gurzhi effect<sup>52</sup>)

$$R \approx R_0 \frac{3\ell_G^2(B)}{W^2} = \frac{3Lm\eta_0}{e^2\rho^{(0)}W^3} \frac{1}{1 + (2\omega_c\tau_{ee})^2}. \quad (12)$$

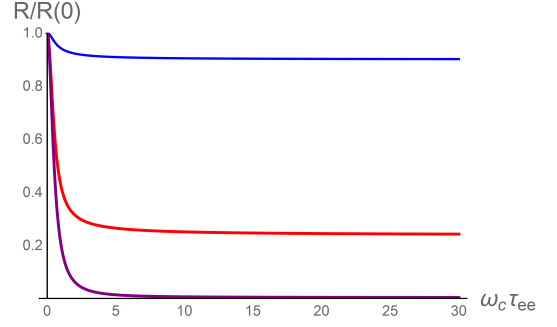


FIG. 2: Resistance in the absence of recombination, Eq. (11b). Different curves (top to bottom) correspond to different values of the ratio  $W/[\ell_G(0)] = 20, 2, 0.2$ .

The resistance (11b) depends on the magnetic field only via the field-dependent viscosity (3). As the field is increased, the viscosity – and hence the Gurzhi length (10) – decreases, leading to *negative* magnetoresistance, see Fig. 2. In the case of a one-component fluid, i.e.  $\tau_{eh} \rightarrow \infty$ , this effect was discussed in Refs. 12,13.

### C. Finite-size sample with recombination

Taking into account electron-hole recombination, we arrive at the following equations

$$\ell_G^2(B)j'' - j + \sigma_0 E + \omega_c \tau_* P = 0, \quad (13a)$$

$$\ell_R^2 P'' - P - \omega_c \tau j = 0, \quad (13b)$$

where the length scale describing the recombination processes is

$$\ell_R = \sqrt{(\eta_{xx} + \langle v^2 \rangle \tau_R / 2) \tau} \approx \sqrt{\langle v^2 \rangle \tau_R \tau / 2} \approx \ell_R(0). \quad (13c)$$

The length  $\ell_R$  does in principle depend on the magnetic field through the field-dependent viscosity, but in the limit of slow recombination this contribution is neglected and the remaining expression does not depend on  $B$ .

In the absence of the magnetic field the equations (13) decouple and we recover our previous results,  $P = 0$  and Eq. (11). In the presence of the magnetic field, the equations (13) allow for a formal solution

$$\begin{pmatrix} j \\ P \end{pmatrix} = \left[ 1 - \cosh(\widehat{M}^{\frac{1}{2}} y) \left[ \cosh(\widehat{M}^{\frac{1}{2}} W/2) \right]^{-1} \right] \begin{pmatrix} j_0 \\ -\omega_c \tau j_0 \end{pmatrix}, \quad (14a)$$

where the matrix  $\widehat{M}$  is given by

$$\widehat{M} = \begin{pmatrix} \ell_G^{-2}(B) & -\omega_c \tau_* \ell_G^{-2}(B) \\ \omega_c \tau \ell_R^{-2}(0) & \ell_R^{-2}(0) \end{pmatrix}. \quad (14b)$$

The spatial variation of the currents is governed by the eigenvalues of the matrix (14b)

$$\lambda_{\pm} = \frac{1}{2} \left[ \ell_G^{-2}(B) + \ell_R^{-2}(0) \right] \pm \sqrt{\left[ \ell_G^{-2}(B) - \ell_R^{-2}(0) \right]^2 / 4 - \ell_G^{-2}(B) \ell_R^{-2}(0) \omega_c^2 \tau \tau_*} \quad (14c)$$

Using the eigenvalues (14c), we express the current  $j$  as

$$j = \frac{j_0}{\lambda_+ - \lambda_-} \left[ \left( 1 - \frac{\cosh \sqrt{\lambda_+} y}{\cosh \sqrt{\lambda_+} W/2} \right) [\ell_G^{-2}(B)(1 + \omega_c^2 \tau \tau_*) - \lambda_-] - \left( 1 - \frac{\cosh \sqrt{\lambda_-} y}{\cosh \sqrt{\lambda_-} W/2} \right) [\ell_G^{-2}(B)(1 + \omega_c^2 \tau \tau_*) - \lambda_+] \right]. \quad (14d)$$

This leads to the following expression for the resistance of the sample

$$R = R_0(\lambda_+ - \lambda_-) \left[ \left( 1 - \frac{2}{\sqrt{\lambda_+} W} \tanh \frac{\sqrt{\lambda_+} W}{2} \right) \left( \ell_G^{-2}(B) - \frac{\lambda_-}{1 + \omega_c^2 \tau \tau_*} \right) - \left( 1 - \frac{2}{\sqrt{\lambda_-} W} \tanh \frac{\sqrt{\lambda_-} W}{2} \right) \left( \ell_G^{-2}(B) - \frac{\lambda_+}{1 + \omega_c^2 \tau \tau_*} \right) \right]^{-1}. \quad (14e)$$

The general expressions (14) can be simplified using the general assumption (5). Indeed, the hydrodynamic approach holds if the electron-electron scattering time  $\tau_{ee}$  is much shorter than any other time scale, including the recombination time. Hence, the Gurzhi length (10) is much smaller than the recombination length (13c):

$$\tau_R \gg \tau_{ee} \Rightarrow \ell_R(0) \gg \ell_G(0).$$

This allows us to expand the square root in Eq. (14c). In this paper, we are interested in the case where the eigenvalues (14c) are real (in general, they may become complex leading to an interesting oscillatory behavior of the currents; this effect will be discussed elsewhere). The necessary condition justifying this assumption is

$$\ell_R(0)/\sqrt{2 + 4\omega_c^2 \tau \tau_*} > \ell_G(B) \quad \text{or} \quad \tau_R \gtrsim \tau_*^2/\tau_{ee}.$$

For simplicity, we will now assume a stronger inequality,

$$\tau_R \gg \tau_*^2/\tau_{ee}. \quad (15)$$

The latter assumption simplifies the algebra, but does not lead to a qualitative change in the results.

Expanding the square root in Eq. (14c), we find

$$\lambda_+ \approx \ell_G^{-2}(B), \quad \lambda_- \approx \frac{1 + \omega_c^2 \tau \tau_*}{\ell_R^2(0)} \equiv \ell_R^{-2}(B). \quad (16)$$

Under the assumptions (16) and (15), the resistance (14e) simplifies and we arrive at the result

$$R = R_0 \left[ \left( 1 - \frac{2\ell_G(B)}{W} \tanh \frac{W}{2\ell_G(B)} \right) - \left( 1 - \frac{2\ell_R(B)}{W} \tanh \frac{W}{2\ell_R(B)} \right) \frac{\omega_c^2 \tau \tau_*}{1 + \omega_c^2 \tau \tau_*} \right]^{-1}. \quad (17)$$

Depending on the parameter values, the expressions (14e) and (17) may exhibit positive, negative, or nonmonotonic magnetoresistance. Below we discuss the emerging parameter regimes.

### III. DISCUSSION

The following discussion of the field dependence of the sample resistance (17) is based on the simple properties of the function

$$f(z) = 1 - \frac{\tanh z}{z} \rightarrow \begin{cases} z^2/3, & z \ll 1, \\ 1 - 1/z, & z \gg 1. \end{cases}$$

#### A. Finite-size sample without recombination

In the absence of recombination (i.e., for  $\ell_R(0) \rightarrow \infty$ ), we may neglect the second term in Eq. (17) and hence recover Eq. (11b).

Using the explicit expression for the viscosity coefficient (3), we re-write the ratio  $\ell_G(B)/W$  as

$$\frac{\ell_G(B)}{W} = \frac{\ell_G(0)}{W} \frac{1}{\sqrt{1 + 4\omega_c^2 \tau_{ee}^2}}.$$

Substituting this expression in Eq. (11b), we find that the magnetoresistance is always *negative* and can be *very large* in strong fields,  $R_{\max}/R_{\min} \gg 1$ .

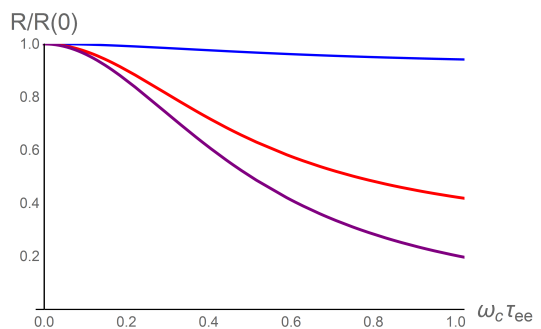


FIG. 3: Resistance in the absence of recombination, Eq. (11b) in weak magnetic fields. Different curves (top to bottom) correspond to different values of the ratio  $W/[\ell_G(0)] = 20, 2, 0.2$ .

The resulting field dependence is shown in Figs. 2 and 3. While the qualitative features of the MR are independent of the particular value of the ratio  $W/\ell_G(0)$ , the effect is much more pronounced in narrow samples.

In weak fields, the MR is quadratic

$$\frac{R(B)}{R(0)} \approx 1 - 2 \left[ \frac{\tanh^2 \frac{W}{2\ell_G(0)}}{1 - \frac{2\ell_G(0)}{W} \tanh \frac{W}{2\ell_G(0)}} - 1 \right] \omega_c^2 \tau_{ee}^2.$$

In very strong fields,  $\omega_c \tau_{ee}, \omega_c \tau_{ee} W/\ell_G(0) \gg 1$ , the resistance saturates approaching the inviscid value  $R_0$ .

The behavior of the system in the absence of recombination is similar to that of the one-component system discussed in Ref. 12. Strictly speaking, the one-component limit is achieved neglecting electron-hole scattering, i.e.,  $\tau_{eh} \gg \tau$ . In this case, the electron and hole subsystems are independent and our system consists of two copies of the system discussed in Ref. 12. At the same time, electron-hole scattering and impurity scattering affect the electric current in the same way. Indeed, the corresponding time scales,  $\tau_{eh}$  and  $\tau$  enter the equation (7c) in a symmetric fashion. As a result, in the absence of recombination the effect of electron-hole scattering is reduced to renormalizing the transport mean free time,  $\tau_*$ .

## B. Finite-size sample with recombination

In the presence of recombination, the magnetoresistance is determined by the interplay between the sample width,  $W$ , and the two length scales,  $\ell_R \gg \ell_G$ . The field dependence of the recombination length  $\ell_R$  is similar to that of the Gurzhi length, however, the typical field scales are rather different:

$$\frac{\ell_R(B)}{W} = \frac{\ell_R(0)}{W} \frac{1}{\sqrt{1 + \omega_c^2 \tau \tau_*}},$$

where under our assumptions

$$\tau \tau_* \gg \tau_{ee}^2.$$

In the absence of the magnetic field, the sample resistance is independent of the weak (under our assumptions) recombination. As a result,  $R(0)$  is the same as above. Furthermore, in the Gurzhi limit (12) this value is independent of  $\tau_{eh}$  as well.

### 1. Weak fields

In weak fields,  $B \rightarrow 0$ , the MR is still quadratic,

$$\frac{R(B)}{R(0)} \approx 1 - A_1 \omega_c^2 \tau_{ee}^2, \quad (18)$$

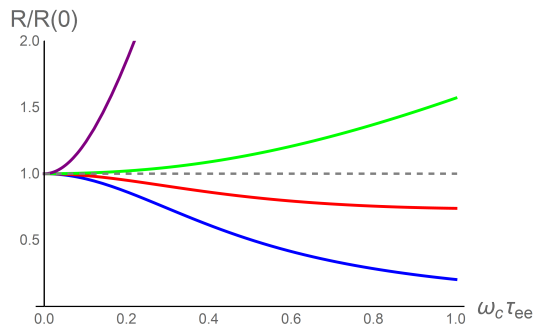


FIG. 4: Resistance (17) in weak magnetic fields. The four curves (top to bottom:  $W/[\ell_G(0)] = 80, 12, 4, 0.1$ ) illustrate the four parameter regimes in Eq. (20). The numerical values correspond to the choice  $\ell_R(0)/\ell_G(0) = 40$ ,  $\tau \tau_*/\tau_{ee}^2 = 100$ .

but with the coefficient that depends on  $\tau_R$ ,  $\tau$ , and  $\tau_*$

$$A_1 = 2 \left[ \frac{\tanh^2 \frac{W}{2\ell_G(0)}}{1 - \frac{2\ell_G(0)}{W} \tanh \frac{W}{2\ell_G(0)}} - 1 \right] - \left[ 1 - \frac{2\ell_R(0)}{W} \tanh \frac{W}{2\ell_R(0)} \right] \frac{\tau \tau_*}{\tau_{ee}^2}.$$

For the narrowest samples,  $W \ll \ell_G(0)$ , the coefficient  $A_1$  is determined by the electron-electron scattering time

$$A_1(W \rightarrow 0) \approx 4,$$

leading to *negative* MR.

For wider samples the coefficient  $A_1$  changes sign. This sign change occurs when

$$W = W_0, \quad W_0^3 \simeq 48 \frac{\tau_{ee}^2}{\tau \tau_*} \ell_R^2(0) \ell_G(0). \quad (19)$$

Hence, for  $W < W_0$ , the MR is still negative, albeit with a smaller coefficient, while for  $W > W_0$  the MR becomes *positive*. For the widest samples,  $W \gg \ell_R(0)$ , we find strong positive MR. The four parameter regimes can be summarized as

$$A_1 \approx \begin{cases} 4, & W \ll \ell_G(0), \\ 4\ell_G(0)/W, & \ell_G(0) \ll W < W_0, \\ -\frac{W^2}{12\ell_R^2(0)} \frac{\tau \tau_*}{\tau_{ee}^2}, & W_0 < W \ll \ell_R(0), \\ -\tau \tau_* \tau_{ee}^{-2}, & W \gg \ell_R(0). \end{cases} \quad (20)$$

The weak-field magnetoresistance (18) is illustrated in Figs. 4 and 5.

### 2. Strong fields

In strong fields,  $B \rightarrow \infty$ , we recover *positive* linear MR<sup>46–48</sup>. This behavior corresponds to the following

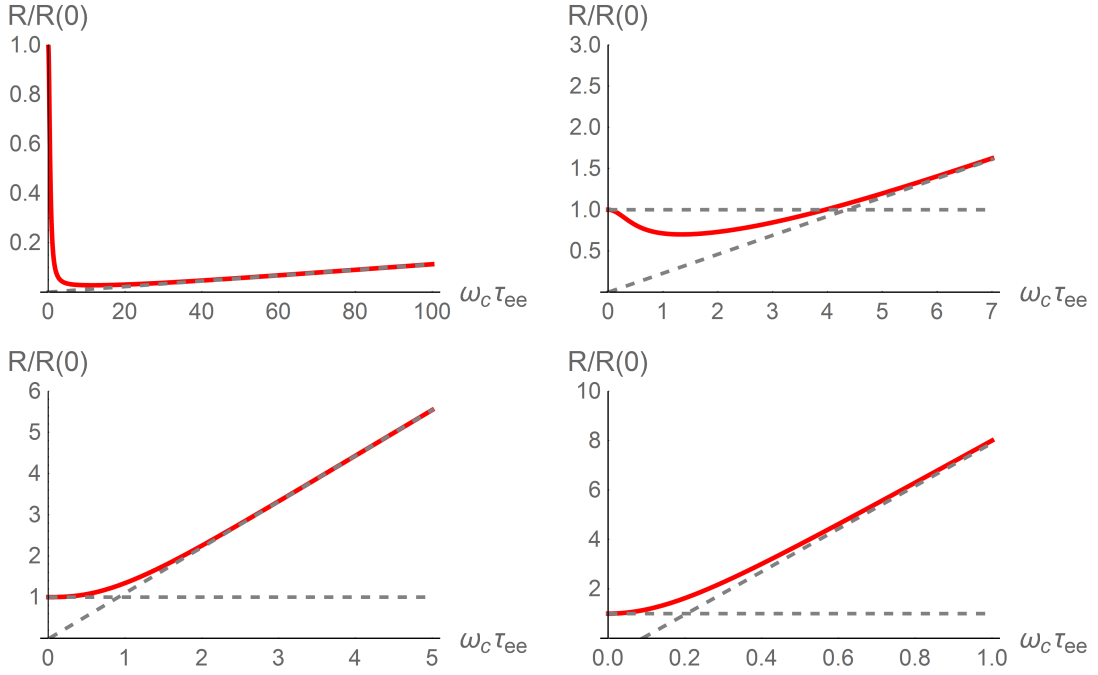


FIG. 5: The four regimes of Eq. (20) illustrated in the four panels (clockwise, from top left:  $W/[\ell_G(0)] = 0.5, 4, 12, 80$ ). The numerical values correspond to the choice  $\ell_R(0)/\ell_G(0) = 50$ ,  $\tau\tau_*/\tau_{ee}^2 = 100$ . The dashed line describes the strong-field limit (21).

regime of parameters:  $\omega_c \tau_{ee} \gg 1$  and  $\omega_c^2 W^2 \tau_* \gg \tau_R \langle v^2 \rangle$ . The resulting resistance is given by

$$\frac{R(B)}{R_0} \approx A_2 \left[ \omega_c \tau_{ee} - A_2 \frac{\tau_{ee}^2}{\tau \tau_*} \right], \quad (21)$$

where

$$A_2 = \frac{W}{2\ell_R(0) \frac{\tau_{ee}}{\sqrt{\tau \tau_*}} - \ell_G(0)}.$$

Here the denominator remains positive as long as the eigenvalues (14c) are real, i.e. for  $\tau_R > \tau_*^2/\tau_{ee}$ . Consequently, in wide samples,  $W > \ell_R(0)$ , the MR is always positive, see Fig. 5 for illustration.

### 3. Intermediate fields

The behavior of the resistance (17) in between the above two asymptotic regimes is strongly affected by the sample width.

In the narrowest samples,  $W \ll \ell_G(0)$ , and not too strong magnetic fields,  $\omega_c \tau_{ee} \ll \sqrt{\tau_* \tau_{ee}}/\tau_B$ , we recover the Gurzhi limit,  $W \ll \ell_G(B)$ , with the Lorentzian-shaped resistance given by Eq. (12). In stronger fields,  $\sqrt{\tau_* \tau_{ee}}/\tau_B \ll \omega_c \tau_{ee} \ll (\tau_{ee}/\tau_B) \sqrt{\tau_R/\tau_*}$ , the width of the sample,  $\ell_G(B) \ll W \ll \ell_R(B)$ , enters the intermediate parameter range. Here, the resistance

$$\frac{R(B)}{R_0} \approx 1 + \frac{\ell_G(0)}{\omega_c \tau_{ee} W} + \frac{\omega_c^2 \tau_{ee} W^2 \tau_*^2}{12\ell_G^2(0) \tau_R}, \quad (22)$$

remains close to its minimum value

$$R_{\min} = R_0 \left[ 1 + \mathcal{O} \left( \tau_*^{2/3} (\tau_R \tau_{ee})^{-1/3} \right) \right] \approx R_0, \quad (23a)$$

that is achieved at

$$\omega_c \rightarrow \omega_c^* = W_0/(2\tau_{ee}W). \quad (23b)$$

In the strongest fields,  $\omega_c \tau_{ee} \gg (\tau_{ee}/\tau_B) \sqrt{\tau_R/\tau_*}$ , the recombination length becomes smaller than the sample width and we recover the above linear MR.

In wider samples, the parameter windows of the above intermediate regimes shrink and gradually disappear, see Fig. 6. For  $\ell_G(0) \ll W \ll \ell_R(0)$ , the condition of the Gurzhi limit is violated and the Lorentzian (12) is no longer a good approximation, while the onset of the intermediate regime (22) is shifted towards weaker fields, see the right panel in Fig. 6. For the widest samples,  $W \gg \ell_R(0)$ , the nonmonotonic behavior disappears and we find positive MR, see the two bottom panels in Fig. 5.

The *nonmonotonic* MR occurs in intermediate-width samples,  $W < W_0$ : it is negative in weak fields, but becomes positive in strong fields. The magnetoresistance (17) is illustrated in Figs. 5 - 7. In particular, the sample resistance as a function of the magnetic field develops a minimum,  $R_{\min} \approx R_0$ , at a particular value of the field,  $B^*$ , see Eqs. (23).

### C. Phase diagram

The expression (17) for the sample resistance shows a rich variety of parameter regimes illustrated in Figs. 4 - 6.

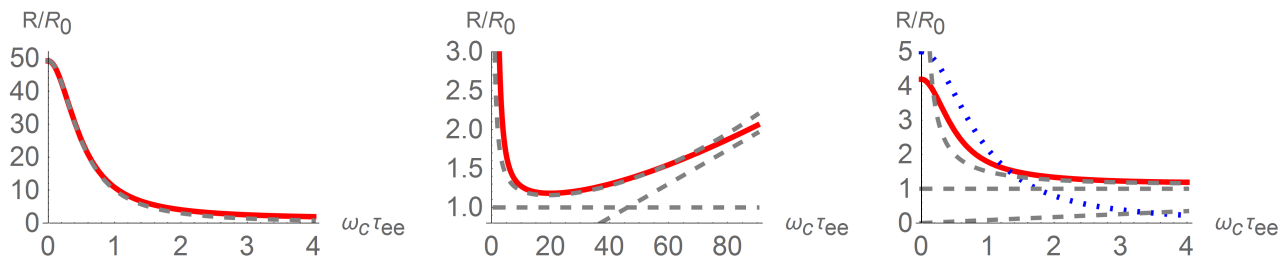


FIG. 6: Intermediate regimes of the resistance. The left panel illustrates the Gurzhi limit in the narrowest samples, Eq. (12), taking into account higher-order corrections in  $W/\ell_G(0)=0.5$  while plotting the Lorentzian (dashed curve). The central panel shows Eq. (22) for the same sample width (dashed curve). The numerical values were computer for  $\ell_R(0)/\ell_G(0)=120$ ,  $\tau\tau_*/\tau_{ee}^2=100$ . The straight dashed line describes the strong-field limit (21). The right panel shows the onset of the intermediate regime (22) for a wider sample with  $W/\ell_G(0)=2$ . The dotted line shows the Lorentzian (12).

The conditions determining these regimes can be summarized in a phase-diagram-like manner, see Fig. 8, where they are shown in terms of the recombination length,  $\ell_R$ , and the sample width represented by the “ballistic” length,  $\tau_B \sim W/\sqrt{\langle v^2 \rangle}$ , see Eq. (5). Under the assumption of the weak recombination adopted in this paper, Eq. (15), the eigenvalues (14c) are real within the whole range of magnetic fields. Varying the sample width with a fixed value of  $\tau_R$ , we may scan through different MR regimes, see Fig. 8.

The narrowest samples are described by the condition  $W \ll \ell_G(0)$ , that can be re-written as  $\tau_B \ll \sqrt{\tau_{ee}\tau_*}$ . In this case, we observe strong negative MR, see the top left panel in Fig. 5. For wider samples,  $\ell_G(0) \ll W < W_0$ , or  $\sqrt{\tau_{ee}\tau_*} \ll \tau_B \ll \tau_R^{1/3}\tau_{ee}^{5/6}\tau_*^{-1/6}$ , the weak field MR is still negative, but is characterized by a small coefficient  $A_1$ , see Eq. (20). In Fig. 8, we refer to this regime as “weak negative MR”. Overall in this regime, the resistance is a *non-monotonic* function of the field: in stronger fields the recombination processes dominate and lead to linear positive MR, see Fig. 7.

Wider samples exhibit positive MR, see the bottom panels in Fig. 5. Since the coefficient  $A_1$  increases drasti-

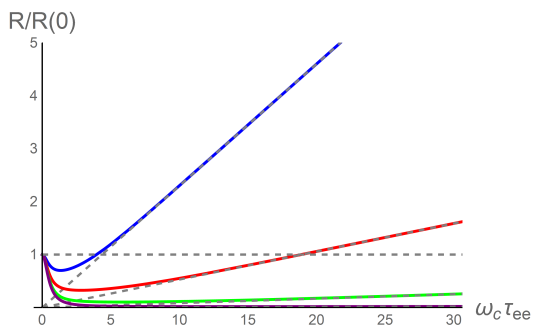


FIG. 7: Nonmonotonic behavior of the resistance (17). Different curves (top to bottom) correspond to different values of the ratio  $W/[\ell_G(0)]=4, 2, 1, 0.4$ . The numerical values correspond to the choice  $\ell_R(0)/\ell_G(0) = 50$ ,  $\tau\tau_*/\tau_{ee}^2 = 100$ . Dashed lines describe the strong-field limit (21).

cally as the width of the sample exceeds the zero-field recombination length. Consequently, we refer to the regime  $\tau_B \gg \sqrt{\tau_R\tau}$  as the regime of strong positive MR in Fig. 8.

Note, that the latter regime disappears in the ultra-clean limit, where formally  $\tau \rightarrow \infty$ . In this case, both eigenvalues  $\lambda_{\pm}$  remain real and finite, although the field-dependent recombination length  $\ell_R(B)$  defined by Eq. (16) becomes inverse proportional to the magnetic field:

$$\ell_R(B) \rightarrow (1/\omega_c)\sqrt{\langle v^2 \rangle \tau_R / (2\tau_{eh})},$$

where we have used the explicit form (13c) of  $\ell_R(0)$  with  $\tau_* \rightarrow \tau_{eh}$ . The resistance (17) simplifies somewhat and becomes

$$\frac{R}{R_0} = \left[ \frac{2}{\omega_c \tau_W} \tanh \frac{\omega_c \tau_W}{2} - \frac{2\ell_G(B)}{W} \tanh \frac{W}{2\ell_G(B)} \right]^{-1}, \quad (24)$$

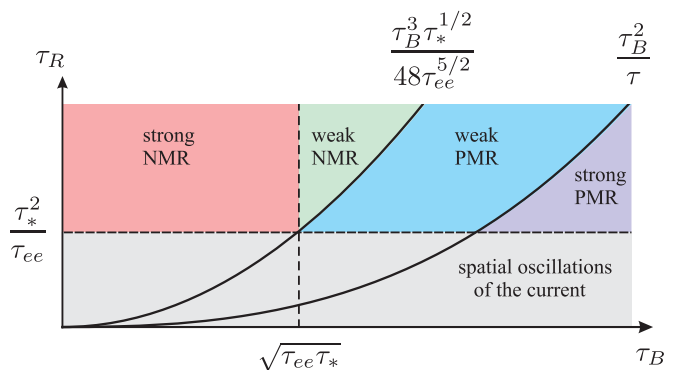


FIG. 8: Summary of the parameter regimes exhibited by the sample resistance subjected to the external magnetic field, Eq. (17). The lower part of the diagram with  $\tau_R \ll \tau_*^2/\tau_{ee}$  describes the regime where the eigenvalues (14c) are complex and the currents exhibit oscillatory behavior. This regime is beyond the scope of this paper and will be addressed elsewhere. The labels “weak/strong NMR (PMR)” refer to the negative (positive) MR in weak magnetic fields, see Eq. (20).



where

$$\tau_W = \tau_B \sqrt{2\tau_{eh}/\tau_R}.$$

In the regime of weak recombination,  $\tau_R \gg \tau_{eh}^2/\tau_{ee}$ , see Eq. (15), the expression (24) exhibits all three regimes shown in the phase diagram, Fig. 8, to the left of the strong positive MR regime.

#### IV. CONCLUSIONS

We considered transport properties of a 2D viscous, two-component electronic liquid at charge neutrality. We showed, that in the narrow strip geometry, the fluid exhibits a Poiseuille-like inhomogeneous flow where the spatial variation of the current density is controlled by the quasiparticle recombination and viscous effects described by the length scales  $\ell_R$  and  $\ell_G$ , respectively, see Fig. 1. Assuming that the recombination length exceeds the viscous Gurzhi length at all fields,  $\ell_R(B) \gg \ell_G(B)$ , we find that the inhomogeneity is strongest near the sample edges.

The contribution of the boundary regions to transport coefficients is strongly affected by the external magnetic field leading to strong, nonmonotonous magnetoresistance. In weak fields, the MR is quadratic in  $B$ , see Eq. (18), and can be positive or negative with the sign change occurring at a particular value of the sample width (19). This behavior is illustrated in Figs. 4 and 8. Depending on parameter values, we distinguish four different regimes of strong and weak, positive and negative MR summarized in Eq. (20).

In strong fields, the MR is positive and linear in  $B^{46-48}$ , see Eq. (21). In the parameter regimes where the weak-field MR is negative, this leads to a nonmonotonic behavior where the resistance curves exhibit a minimum (23) at a particular value of the field,  $B^*$ , see Figs. 4 and 7.

In this paper we have considered the electronic system in the hydrodynamic regime. Any temperature dependence of transport coefficients appears by means of

the temperature dependence of the scattering times  $\tau_{ee}$ ,  $\tau_{eh}$ , and  $\tau_R$ . This temperature dependence is beyond the scope of the hydrodynamic approach and has to be derived from a microscopic theory (see, e.g. Ref. 58 for such derivation in graphene). We have assumed, see Eq. (5), that intra-band scattering is more effective than inter-band scattering, i.e.  $\tau_{eh} \gg \tau_{ee}$ . While this can be easily achieved in double-layer electron-hole structures<sup>59</sup>, we believe that at the qualitative level our results are unaffected by this assumption and remain valid in a more general case where  $\tau_{eh} \sim \tau_{ee}$ . We have also neglected the effects of the Hall viscosity, see discussion in the text between Eqs. (6) and (7). Indeed, the shortest length scale describing spatial variation of the current is  $\xi \sim \ell_G(B)$ . In this case, the smallness of the Hall viscosity terms (in comparison to the Lorentz terms) in Eqs. (6) is justified by our main assumption (5).

The effects described in this paper can be observed experimentally in any 2D compensated semimetal, including graphene, topological insulators, and narrow band semiconductors. Recently, the hydrodynamic behavior has been observed in Weyl semimetals<sup>11</sup>. These materials are three-dimensional and show the behavior discussed in this paper in the case where the current is perpendicular to the magnetic field<sup>11</sup>. In the inviscid limit, neutral 3D systems with the slab geometry behave very similarly to 2D systems<sup>48</sup>. We expect that our present results for viscous two-fluid flows are applicable in this case as well.

#### Acknowledgments

We thank M.I. Dyakonov, A.D. Mirlin, D.G. Polyakov, J. Schmalian, and M. Schütt for fruitful discussions. This work was supported by the Dutch Science Foundation NWO/FOM 13PR3118 (MT), the Russian Foundation for Basic Research Grant 17-02-00217 (VYK), the Russian Science Foundation Grant 17-12-01182 (PSA, APD, IVG), and the MEPhI Academic Excellence Project, Contract No. 02.a03.21.0005 (BNN).

<sup>1</sup> R.P. Feynman, R.B. Leighton, and M. Sands, *The Feynman Lectures on Physics* (Basic Books, New York, 2011).

<sup>2</sup> N.W. Ashcroft and N.D. Mermin, *Solid State Physics* (Holt, Rinehart and Winston, New York, 1976).

<sup>3</sup> B. N. Narozhny, I. V. Gornyi, A. D. Mirlin, and J. Schmalian, *Annalen der Physik* (2017).

<sup>4</sup> D. A. Bandurin, I. Torre, R. Krishna Kumar, M. Ben Shalom, A. Tomadin, A. Principi, G. H. Auton, E. Khestanova, K. S. Novoselov, I. V. Grigorieva, L. A. Ponomarenko, A. K. Geim, and M. Polini, *Science* **351**, 1055 (2016).

<sup>5</sup> J. Crossno, J.K. Shi, K. Wang, X. Liu, A. Harzheim, A. Lucas, S. Sachdev, P. Kim, T. Taniguchi, K. Watanabe, T.A. Ohki, and K.C. Fong, *Science* **351**, 1058 (2016).

<sup>6</sup> R. Krishna Kumar, D. A. Bandurin, F. M. D. Pelle-

grino, Y. Cao, A. Principi, H. Guo, G. H. Auton, M. Ben Shalom, L. A. Ponomarenko, G. Falkovich, K. Watanabe, T. Taniguchi, I. V. Grigorieva, L. S. Levitov, M. Polini, and A. K. Geim, *Nature Physics* (2017).

<sup>7</sup> P.J.W. Moll, P. Kushwaha, N. Nandi, B. Schmidt, and A.P. Mackenzie, *Science* **351**, 1061 (2016).

<sup>8</sup> L. Bockhorn, P. Barthold, D. Schuh, W. Wegscheider, and R. J. Haug, *Phys. Rev. B* **83**, 113301 (2011).

<sup>9</sup> R.G. Mani, A. Kriisa, and W. Wegscheider, *Sci. Rep.* **3**, 2747 (2013).

<sup>10</sup> Q. Shi, P.D. Martin, Q.A. Ebner, M.A. Zudov, L.N. Pfeiffer, and K.W. West, *Phys. Rev. B* **89**, 201301 (2014).

<sup>11</sup> J. Gooth, F. Menges, C. Shekhar, V. Süß, N. Kumar, Y. Sun, U. Drechsler, R. Zierold, C. Felser, and B. Gotsmann, arXiv:1706.05925 (2017).

- <sup>12</sup> P.S. Alekseev, Phys. Rev. Lett. **117**, 166601 (2016).
- <sup>13</sup> T. Scaffidi, N. Nandi, B. Schmidt, A. P. Mackenzie, and J. E. Moore, Phys. Rev. Lett. **118**, 226601 (2017).
- <sup>14</sup> A. L. Friedman, J. L. Tedesco, P. M. Campbell, J. C. Culbertson, E. Aifer, F. K. Perkins, R. L. Myers-Ward, J. K. Hite, C. R. Eddy, G. G. Jernigan, and D. K. Gaskill, Nano Lett. **10**, 3962 (2010).
- <sup>15</sup> R. S. Singh, X. Wang, W. C. Ariando, and A. T. S. Wee, App. Phys. Lett. **101**, 183105 (2012).
- <sup>16</sup> M. Veldhorst, M. Snelder, M. Hoek, C. G. Molenaar, D. P. Leusink, A. A. Golubov, H. Hilgenkamp, and A. Brinkman, Phys. Stat. Solidi RRL **7**, 26 (2013).
- <sup>17</sup> W. Wang, Y. Du, G. Xu, X. Zhang, E. Liu, Z. Liu, Y. Shi, J. Chen, G. Wu, and X. Zhang, Sci. Rep. **3**, 2181 (2013).
- <sup>18</sup> G. M. Gusev, E. B. Olshanetsky, Z. D. Kvon, N. N. Mikhailov, and S. A. Dvoretzky, Phys. Rev. B **87**, 081311 (2013).
- <sup>19</sup> F. Kisslinger, C. Ott, C. Heide, E. Kampert, B. Butz, E. Spiecker, S. Shallcross, and H. B. Weber, Nature Phys. **11**, 650 (2015).
- <sup>20</sup> S. Wiedmann, A. Jost, C. Thienel, C. Brune, P. Leubner, H. Buhmann, L. W. Molenkamp, J. C. Maan, and U. Zeitler, Phys. Rev. B **91**, 205311 (2015).
- <sup>21</sup> C. M. Wang and X. L. Lei, Phys. Rev. B **92**, 125303 (2015).
- <sup>22</sup> G. Yu. Vasileva, D. Smirnov, Yu. L. Ivanov, Yu. B. Vasilyev, P. S. Alekseev, A. P. Dmitriev, I. V. Gornyi, V. Yu. Kachorovskii, M. Titov, B. N. Narozhny, and R. J. Haug, Phys. Rev. B **93**, 195430 (2016).
- <sup>23</sup> X. Wang, Y. Du, S. Dou, and C. Zhang, Phys. Rev. Lett. **108**, 266806 (2012).
- <sup>24</sup> O. Pavlosiuk, D. Kaczorowski, and P. Wisniewski, Sci. Rep. **5**, 9158 (2015).
- <sup>25</sup> M. N. Ali, J. Xiong, S. Flynn, J. Tao, Q. D. Gibson, L. M. Schoop, T. Liang, N. Haldolaarachchige, M. Hirschberger, N. P. Ong, and R. J. Cava, Nature (London) **514**, 205 (2014).
- <sup>26</sup> I. Pletikoscic, M. N. Ali, A. V. Fedorov, R. J. Cava, and T. Valla, Phys. Rev. Lett. **113**, 216601 (2014).
- <sup>27</sup> C. Shekhar, A. K. Nayak, Y. Sun, M. Schmidt, M. Nicklas, I. Leermakers, U. Zeitler, Z. Liu, Y. Chen, W. Schnelle, J. Grin, C. Felser, and B. Yan, Nature Phys. **11**, 645 (2015).
- <sup>28</sup> N. Kumar, C. Shekhar, S.-C. Wu, I. Leermakers, O. Young, U. Zeitler, B. Yan, and C. Felser, Phys. Rev. B **93**, 241106 (2016).
- <sup>29</sup> T. Liang, Q. Gibson, M. N. Ali, M. Liu, R. J. Cava, and N. P. Ong, Nat. Mater. **14**, 280 (2015).
- <sup>30</sup> K. Gopinadhan, Y. J. Shin, R. Jalil, T. Venkatesan, A. K. Geim, A. H. Castro Neto, and H. Yang, Nat. Commun. **6**, 8337 (2015).
- <sup>31</sup> F. Arnold, C. Shekhar, S.-C. Wu, Y. Sun, R. D. dos Reis, N. Kumar, M. Naumann, M. O. Ajeesh, M. Schmidt, A. G. Grushin, J. H. Bardarson, M. Baenitz, D. Sokolov, H. Bormann, M. Nicklas, C. Felser, E. Hassinger, and B. Yan, Nat. Commun. **7**, 11615 (2015).
- <sup>32</sup> C.-L. Zhang, S.-Y. Xu, I. Belopolski, Z. Yuan, Z. Lin, B. Tong, N. Alidoust, C.-C. Lee, S.-M. Huang, T.-R. Chang, H.-T. Jeng, H. Lin, M. Neupane, D. S. Sanchez, H. Zheng, G. Bian, J. Wang, C. Zhang, H.-Z. Lu, S.-Q. Shen, T. Neupert, M. Z. Hasan, and S. Jia, Nat. Commun. **7**, 10735 (2016).
- <sup>33</sup> H. Li, H. He, H.-Z. Lu, H. Zhang, H. Liu, R. Ma, Z. Fan, S.-Q. Shen, and J. Wang, Nat. Commun. **7**, 10301 (2016).
- <sup>34</sup> Y. Luo, R. D. McDonald, P. F. S. Rosa, B. Scott, N. Wakeham, N. J. Ghimire, E. D. Bauer, J. D. Thompson, and F. Ronning, Sci. Rep. **6**, 27294 (2016).
- <sup>35</sup> M. Diez, A. M. R. V. L. Monteiro, G. Mattoni, E. Cobanera, T. Hyart, E. Mulazimoglu, N. Bovenzi, C. W. J. Beenakker, and A. D. Caviglia, Phys. Rev. Lett. **115**, 016803 (2015).
- <sup>36</sup> D. T. Son and B. Z. Spivak, Phys. Rev. B **88**, 104412 (2013).
- <sup>37</sup> A. A. Burkov, Phys. Rev. B **91**, 245157 (2015); J. Phys.: Cond. Mat. **27**, 113201 (2015).
- <sup>38</sup> B. Z. Spivak and A. V. Andreev, Phys. Rev. B **93**, 085107 (2016).
- <sup>39</sup> A. Lucas, R. A. Davison, and S. Sachdev, PNAS **113**, 9463 (2016).
- <sup>40</sup> S. L. Adler, Phys. Rev. **177**, 2426 (1969).
- <sup>41</sup> J. S. Bell and R. Jackiw, Il Nuovo Cimento A **60**, 47 (1969).
- <sup>42</sup> H. Nielsen and M. Ninomiya, Physics Letters B **130**, 389 (1983).
- <sup>43</sup> M. M. Parish and P. B. Littlewood, Nature (London) **426**, 162 (2003).
- <sup>44</sup> A. A. Abrikosov, Zh. Eksp. Teor. Fiz. **56**, 1391 (1969) [Sov. Phys. JETP **29**, 746 (1969)]; Phys. Rev. B **58**, 2788 (1998); Europhys. Lett. **49**, 789 (2000).
- <sup>45</sup> J. Klier, I. V. Gornyi, and A. D. Mirlin, Phys. Rev. B **92**, 205113 (2015); arXiv:1709.02361 (2017).
- <sup>46</sup> B. N. Narozhny, I. V. Gornyi, M. Titov, M. Schütt, and A. D. Mirlin, Phys. Rev. B **91**, 035414 (2015).
- <sup>47</sup> P. S. Alekseev, A. P. Dmitriev, I. V. Gornyi, V. Y. Kachorovskii, B. N. Narozhny, M. Schütt, and M. Titov, Phys. Rev. Lett. **114**, 156601 (2015).
- <sup>48</sup> P. S. Alekseev, A. P. Dmitriev, I. V. Gornyi, V. Y. Kachorovskii, B. N. Narozhny, M. Schütt, and M. Titov, Phys. Rev. B **95**, 165410 (2017).
- <sup>49</sup> P. S. Alekseev, I. V. Gornyi, A. P. Dmitriev, V. Yu. Kachorovskii, and M. A. Semina, Semiconductors **51**, 766 (2017).
- <sup>50</sup> L. D. Landau and E. M. Lifshitz, *Fluid Mechanics* (Butterworth-Heinemann, Oxford, UK, 2000).
- <sup>51</sup> J. L. M. Poiseuille, C. R. Acad. Sci. **11**, 961 (1840).
- <sup>52</sup> R. N. Gurzhi, Zh. Eksp. Teor. Fiz. **44**, 771 (1963), [Sov. Phys. JETP **17**, 521 (1963)]; Usp. Fiz. Nauk **94**, 689 (1968), [Sov. Phys. Usp. **11**, 255 (1968)].
- <sup>53</sup> H. Guo, E. Ilseven, G. Falkovich, and L. S. Levitov, PNAS **114**, 3068 (2017).
- <sup>54</sup> M. Knudsen, Annalen der Physik **333**, 75 (1909).
- <sup>55</sup> M. Titov, R. V. Gorbachev, B. N. Narozhny, T. Tudorovskiy, M. Schütt, P. M. Ostrovsky, I. V. Gornyi, A. D. Mirlin, M. I. Katsnelson, K. S. Novoselov, A. K. Geim, and L. A. Ponomarenko, Phys. Rev. Lett. **111**, 166601 (2013).
- <sup>56</sup> The case of linear spectrum in, e.g., graphene or 2D surface of 3D topological insulators will be considered elsewhere. At the qualitative level, however, we expect that the main conclusions of this paper will hold even in this special case.
- <sup>57</sup> M. S. Steinberg, Phys. Rev. **109**, 1486 (1958).
- <sup>58</sup> U. Briskot, M. Schütt, I. V. Gornyi, M. Titov, B. N. Narozhny, and A. D. Mirlin, Phys. Rev. B **92**, 115426 (2015).
- <sup>59</sup> For references on double-layer structures see, e.g., B. N. Narozhny and A. Levchenko, Rev. Mod. Phys. **88**, 025003 (2016).